RSC Advances

Journal Name

ARTICLE TYPE

Different interaction between metal electrode and organic layer and their different electrical bistability performances

Yong Ma[a], Pei-Yang Gu[a], Feng Zhou[a], Hui-Long Dong[b], You-Yong Li[b], Qing-Feng Xu [a],*, Jian-Mei Lu [a],*, Wan-Li Ma[b]

A new *p-π* conjugated small molecule 2-[(Pyridin-4-ylmethylene)-amino]-6-(N'-pyridin-4-ylmethylene-hydrazino)-benzo[*de*]isoquinoline-1,3-dione (**2PyNI**) was synthesized, characterized and fabricated into memory devices. Device ITO/**2PyNI**/Au (**1**) showed volatile memory effect, while device ITO/**2PyNI**/Al
10 (**2**) showed Write Once Read Many times (WORM) effect. According to the theoretical calculation, **2PyNI** had different interaction with metal Au and Al, which produced the different memory behavior of device **1** and **2** respectively. In addition, the I-V characteristics of device **1** and **2** were analyzed in detail with various conduction models. The temperature dependence of the current for ON state of device **1** and **2** were performed. Under the irradiation of the UV light (365 nm), device **1** could be switched on
15 automatically when the voltage was fixed at -3.0 V and switched off as the bias was removed.

Introduction

Organic materials are expected to be widely applied in light-emitting diodes, solar cells and high density data storage (HDDS) memory devices.[1-6] To memory devices, different memory types
20 based on organic materials have been obtained through changing the active layer, such as non-volatile Write Once Read Many times (WORM), Flash (rewritable) and volatile Dynamic Random Access Memory (DRAM) etc.[7-9] To tune the suitable memory types is important for future practical application. There're
25 several reported methods such as adjustment of the component ratio of polymer composites and modification of molecular structure. For instance, Chen *et al.* once fabricated memory devices from Flash to WORM memory behavior only tuning the ratio of polyimide and the additive, graphene oxide.[10] In our
30 previous study, an aromatic hydrazone, SNACA ([3-(N-butyl-4-carbaldehyde-1,8-naphthalimide)-9-hexyl ether-9Hcarbazole]) showed voltile memory behavior (DRAM) when fabricated as a ITO or Pt/SNACA film/Al memory device. However, changing the hydrazone linker by a linear *π*-spacer, pyridyl acetylene, the
35 organic compound CAPyNA based device showed a different WORM memory performance.[11] However, the factors affecting the performances of the organic devices are far from the organic layer itself. The interfaces between active layer and metal electrode layer also played an important role to the memory
40 behavior.[12-16] For example, it is well known that the organic molecule has different interaction with various metal layers. Most studies showed that ON/OFF ratio and switching voltage could be influenced by the electrodes, however, the memory types were seldom to be changed .[17-19]

45 Here, we fabricated devices with different metal electrodes intended to study the relationship of memory behaviour and the interface of and organic layer. A new *p-π* conjugated molecule 2-[(Pyridin-4-ylmethylene)-amino]-6-(N'-pyridin-4-ylmethylene-hydrazino)-benzo[*de*]isoquinoline-1,3-dione (**2PyNI**) based on
50 the well-known backbone, naphthalimide and hydrazone, having been widely studied for its excellent photoelectric properties.[20,21] Moreover, pyridines were introduced at the edge of molecule, which was easy to interact with metal for its inherent flexibility in being able to bind through the nitrogen atom or the *π*-ring.
55 According to the theoretical simulation, **2PyNI** had different interaction with metal Au and Al. When two devices ITO/**2PyNI**/Au (**1**) and ITO/**2PyNI**/Al (**2**) were fabricated, their current-voltage chacteristics showed expectedly different memory types, in which device **1** showed volatile memory performance
60 and device **2** showed non-volatile WORM effect. Besides, the OFF (low-conductivity) state of the I-V characteristics for device **1** and **2** could be fitted with various conduction models. Moreover, device **1** could be switched on by irradiation of UV light. We speculated the mechanism by using the theoritical
65 calculation, experimental characterization and conduction models.

Experimental

Materials

4-bromo-1,8-naphthalic anhydride (97%, Liaoning Liangang Dyes Chemical Co. Ltd., China), hydrazine hydrate (85%,
70 Sinopharm Chemical Reagent), pyridine-4-carbaldehyde (97%, TCI), sodium hydroxide (96%, Shanghai Sinopharm), acetic acid (99%, Shanghai Sinopharm) were purchased from commercial

sources.

Apparatus

^{1}H NMR spectra were measured on an INOVA 400 MHz FT-NMR spectrometer, using $CDCl_3$ or DMSO-d_6 as solvent and tetramethylsilane (TMS) as the internal standard at ambient temperature. The UV-vis absorption spectra were recorded on a Perkin Elmer Lambda-17 spectrophotometer at room temperature. Thermogravimetric analysis (TGA) was conducted on a TA instrument Dynamic TGA 2950 at a heating rate of 20 ℃ min^{-1} under a nitrogen flow rate of 100 mL min^{-1}. The fluorescence spectra were measured on Edinburgh-920 fluorescence spectra photometer (Edinburgh Co. UK) with a slit of 3 nm. The fluorescent quantum yield (QY) in the solution was determined using fluorescein (Φ_F = 79 % in 0.1 mmol L^{-1} NaOH) as standard. Cyclic voltammetry was performed at room temperature using an ITO working electrode, a reference electrode Ag/AgCl, and a counter electrode (Pt wire) at a sweep rate of 100 mV s^{-1} (CorrTest CS Electrochemical Workstation analyzer) in a solution of tetra-butylammonium hexafluorophosphate (TBAP) in CH_3CN (0.1 mmol L^{-1}). The scanning electron microscopy (SEM) images were taken on a Hitachi S-4700 scanning electron microscope. The atomic force microscopy (AFM) measurements were performed by using a MFP-3DTM (Digital Instruments/Asylum Research) AFM instrument in the tapping mode. The single crystal X-ray diffraction was made on Rigaku Mercury CCD X-ray diffractometer (50 KV, sealed tube) at 223 K using graphite monochromated Mo Kα and a suitable single crystal mounted at the top of a glass fiber. Diffraction data was collected in ω mode and reduced using the program CrystalClear and the application of a semi-empirical absorption correction. The reflection data was further corrected for Lorentz and polarization effects. The elemental analysis (EA) of C, H and N was performed by the Elemental Analysis Service using an EA1110-CHNS elemental analyzer.

Synthesis of compounds

Synthesis of N-amino-4-hydrazine-1, 8 naphthalimide (1) was according to the references.[22,23] The product was characterized by ^{1}H NMR (DMSO-d_6, 400 MHz) δ (ppm): 9.18 (s, 1H), 8.61 (d, J = 8.4 Hz, 1H), 8.41 (d, J = 7.2 Hz, 1H), 8.27 (d, J = 8.8 Hz, 1H), 7.62 (t, J = 7.6 Hz, 8.0 Hz, 1H), 7.22 (d, J = 8.4 Hz, 1H), 5.70 (s, 2H), 4.68 (s, 2H).

Synthesis of 2-[(Pyridin-4-ylmethylene)-amino]-6-(N'-pyridin-4-ylmethylene-hydrazino)-benzo[de]isoquinoline-1,3-dione (2PyNI): Compound 1 (1.2 g, 5.0 mmol), pyridine-4-carbaldehyde (1.2 g, 12 mmol) and a catalytic amount of acetic acid were dissolved in 150 mL anhydrous ethanol and heated to reflux for 8 h. The precipitate was filtered off and washed three times with anhydrous ethanol (10 mL). Recrystallization from mixed solvent of DMF (N,N-dimethyl-formamide) and acetonitrile (volume ratio is 1:1) gave **2PyNI**. Yellow solid (1.6 g, 3.8 mmol, yield, 76%) was obtained. EA: Calcd for $C_{24}H_{16}N_6O_2$ (%): C, 68.56; H, 3.84; N, 19.99; found: C, 68.41; H, 3.94; N, 19.78. ^{1}H NMR (DMSO-d_6, 400 MHz) δ (ppm): 11.81 (s, 1H), 8.87 (s, 1H), 8.84 (d, J = 8.9 Hz, 2H), 8.81 (s, 1H), 8.65 (d, J = 5.4 Hz, 2H), 8.53 (d, J = 7.2 Hz, 1H), 8.42 (d, J = 8.2 Hz, 2H), 7.89 (s, 1H), 7.88 (s, 1H), 7.84 (dd, J = 8.1, 4.3 Hz, 2H), 7.75 (d, J = 5.6 Hz, 2H). ^{13}C NMR (400 MHz, CF_3COOD) δ (ppm): 189.66, 153.38, 153.16, 150.56, 148.51, 147.66, 146.52, 143.43, 141.80, 140.70, 140.63, 137.37, 136.72, 136.48, 136.38, 134.76, 134.53, 131.18, 129.55, 129.40, 126.59, 126.49, 123.51, 123.31. HRMS-ESI (m/z): [M+H]$^+$ Calcd for $C_{24}H_{17}N_6O_2$, 421.1408, found, 421.1407.

Fabrication of memory devices

The indium tin oxide (ITO) glass was pre-cleaned sequentially with deionized water, acetone and ethanol in an ultrasonic bath, each for 20 min. The active organic film was deposited on the ITO-glass substrate under high vacuum (~10^{-6} Torr). The film was annealed at 70 °C in a vacuum oven for 12 h. Al or Au layer (~50 nm) was thermally evaporated and deposited onto the organic surface at ~10^{-5} Torr through a shadow mask to form the top electrode. The active area of the fabricated device was 0.126 mm^2 (a nummular point with a radius of 0.2 mm). The MoO_3 layer added in the device was deposited on the **2PyNI** film under high vacuum (~10^{-6} Torr). All electrical measurements of the device were characterized under ambient conditions, without any encapsulation, using a HP4145B semiconductor parameter analyzer.
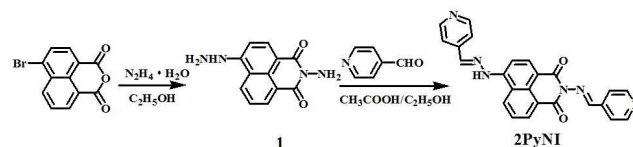
Scheme 1. The synthesis and chemical structure of **2PyNI**

Results and discussion

The product of **2PyNI** was characterized by HNMR, IR and CCD X-ray diffractometer. The thermal stability of **2PyNI** was evaluated by TGA under a nitrogen atmosphere. As shown in the TGA curves (Figure S3), the thermal decomposition temperature (the 5% weight-lost temperature) of **2PyNI** was up to 297 ^{o}C. The good-thermal stability of **2PyNI** would endure heat deterioration in the memory devices. The X-ray diffraction (XRD) measurement showed no obvious peak indicating the amorphous structure of **2PyNI** film deposited by thermal vacuum deposition.

Crystal structure of 2PyNI

Single crystal of 2PyNI·2H$_2$O were obtained by slow evaporation of DMF solution (the key parameters of crystal structure were listed in Table S1). In its asymmetric unit, there were one **2PyNI** and two water molecules. The naphalamide ring and two pyridine rings linked via two hydrazone bridges in different modes. The dihedral angle of naphalamide and pyridine in planar conformation was 5.536° while that in distorted conformation is 83.459°. Figure 1 showed the molecular packing view. There was π-π stacking (3.382 Å) between nearby naphalamide rings. Due to the existence of water molecules, hydrogen bondings enclose the molecules into a 3-D supramolecular structure.
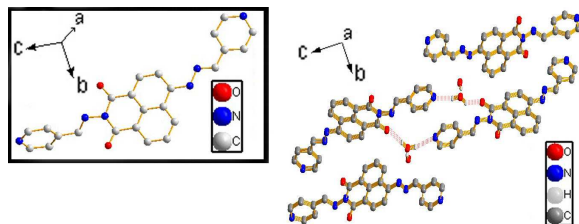
Figure 1. Crystal structure of 2PyNI and 3-D stacking patterns of 2PyNI viewed along *a* axis (hydrogen bonds are denoted by red dotted lines) and hydrogen atoms were omitted for clarification.

Optical properties of 2PyNI
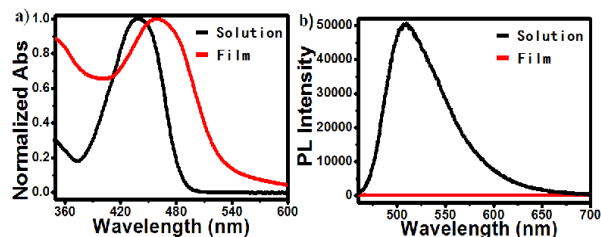
Figure 2. (a) UV–Vis absorption spectrum of 2PyNI in THF solution (black) and film (red); (b) The fluorescence emission spectrum of 2PyNI in THF solution and film with the excitation wavelength 460 nm.

The UV–Vis absorption spectrum of **2PyNI** in dilute tetrahydrofuran (THF) solution displayed one major absorption peak at 438 nm, which was assigned to the π-π^* transition in the naphthalimide moieties.[24,25] The absorption spectrum of **2PyNI** film on quartz substrate showed a visible bathochromic-shift (from 438 to 461 nm) and broadened absorption band (Figure 2a), suggesting the formation of molecular aggregation and/or increased polarity of the thin film.[26-28] This was beneficial for the improvement of the charge carrier mobility of the films.[29] The fluorescent emission spectrum of **2PyNI** in THF solution was 525 nm with quantum yield of 60%. The fluorescent quantum yield (QY) in the solution was determined using fluorescein (Φ_F = 79 % in 0.1 M NaOH) as standard. The fluorescence of **2PyNI** film on quartz substrate was quenched, also assigned to the molecule aggregation.

Electrochemical properties of 2PyNI

The highest occupied molecular orbital (HOMO) and lowest unoccupied molecular orbital (LUMO) energy levels could be calculated from the UV-Vis absorption spectrum and the cyclic voltammetry (CV) results *via* the following equations:

$$E_{HOMO} = -\left[E_{OX}(onset) + 4.80 - E_{Foc}\right]$$

$$E_{LUMO} = E_{HOMO} + E_g$$

where $E_{OX}^{(onset)}$ was the onset oxidation potential, E_{Foc} was the external standard potential of the ferrocene/ferrocenium ion couple and E_g was the band gap determined from UV-Vis absorption spectrum. The optical band gap of **2PyNI** film, estimated from absorption edges, was 2.54 eV (Figure 2a). The onset oxidation $E_{OX}^{(onset)}$ of **2PyNI** film was 1.12 eV (Figure 3). The E_{Foc} was 0.50 eV, as determined from CV measurement with bare ITO glass substrate without molecule film. Assuming that the HOMO level for the Fc/Fc+ standard was -4.80 eV with

respect to the zero vacuum level, the HOMO level for **2PyNI** film is determined to be -5.4 eV. Thus, the LUMO level was estimated to be -2.9 eV. The energy barrier between the work functions (Φ) of the ITO (-4.8 eV) and HOMO energy level (-5.4 eV) was 0.6 eV, which was much lower than the energy barrier between the Φ of the Al (-4.3 eV) or Au (-5.2 eV) and the LUMO energy level (-2.9 eV). This indicated that hole injection from ITO into the HOMO of **2PyNI** (corresponding to ITO as the anode) was easier than electron injection from Al or Au into the LUMO of **2PyNI** (Figure 6b). Thus, the hole-injection predominated the conduction process to the film of **2PyNI**.[30]
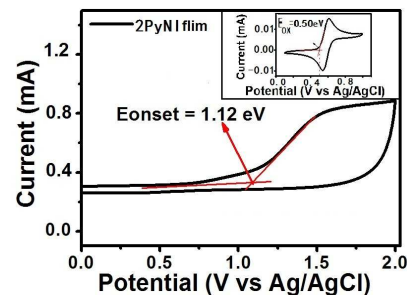
Figure 3. Cyclic voltammograms of 2PyNI film was measured in 0.1 mmol L^{-1} TBAP/CH$_3$CN solution with Ag/AgCl as reference electrode and Pt wire as counter electrode. A scan rate of 100 mV s-1 was used.

Morphology of 2PyNI

Atomic force microscopy (AFM) was used to characterize the surface morphologies and roughness of the vacuum-deposited electroactive layers. The surface root-mean-square roughness of **2PyNI** film was 0.821 nm (Figure 4). The small surface roughness in the AFM image of the film led to the good quality of the film, which could offer a strong guarantee for high performance data-storage devices.
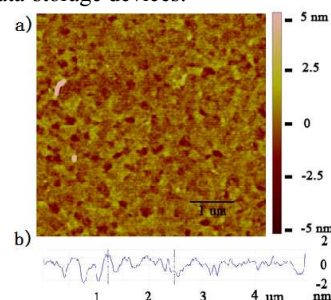
Figure 4. Tapping-mode AFM height images of thin film spin-coating onto ITO substrates annealed at 70 ℃; (a) morphology for 2PyNI; (b) roughness of 2PyNI film.

Electrochemical properties of memory devices

The current-voltage (I-V) characteristic of **2PyNI** in device **1** was shown in Figure 5a. When a voltage sweep was applied from 0 V to -6 V (sweep 1), the device was initially in the low-conductivity (OFF) state. As the negative bias increased further, the memory device switched from the OFF state to the high-conductivity (ON) state at the voltage of -4.3 V, as was indicated by the abrupt increase of the current from 10^{-5} A to 10^{-1} A. The transition from the OFF state to the ON state could serve as the "write" process. The device remained in ON state during the subsequent scan from 0 to -6V (sweep 2) and 0 to 6V (sweep 3). Subsequent application of the negative scan from 0 to -6V (sweep 4) was performed after turning off power for about 2 min, device **1** could be

reprogrammed from the OFF state to the ON state at -4.2 V again. The OFF state could be further written to the ON state when the voltage was reapplied, indicating that the memory device was rewritable and volatile. The short retention time of the ON state
5 suggested that device **1** showed the volatile memory characteristic.[31]
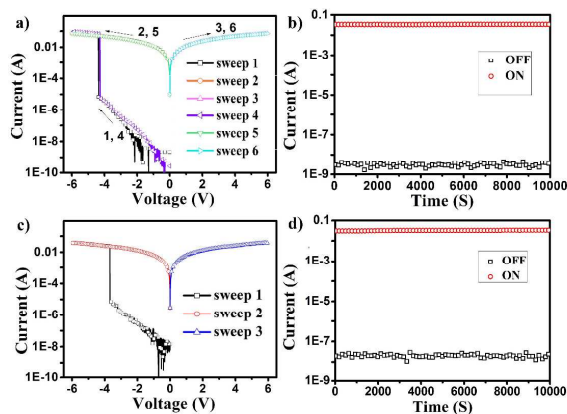
Figure 5. (a, c) Current-voltage (I-V) characteristics of the 2PyNI memory device; (b, d) The effect of retention time of the memory device
10 under a constant stress of -1.0 V.

The current-voltage characteristic of device **2** was shown in Figure 5c. The device switched at a threshold voltage of -3.8 V with the current from 10^{-5} A to 10^{-1} A (sweep 1). The ON state was still observed during the subsequent voltage sweep (sweep 2
15 and sweep 3), even though the voltage was withdrawn for longer time. Thus, the non-volatile memory behavior of device **2** showed the characteristic of WORM memory performance.[32]

At a constant stress of -1.0 V, no obvious degradation in the current for the OFF and ON states of devices **1** and **2** were
20 observed during the long-term testing of about 10^4 s (Figure 5b, d). The results suggested the excellent device stability.

Calculation details and mechanisms

To further understand the different memory behaviours due to the different top electrode, we first utilized the theoretical calculation
25 to illustrate the interaction of organic molecule and metal electrodes. All calculations based on density functional theory (DFT) with generalized gradient approximation (GGA) were implemented in DMol^3 code available in Materials Studio 6.0.[33] For the calculation, Au13 cluster was chosen as a representative
30 of the gold layer, which was seen as a gold "magic" number cluster and used as the adsorptive of organic molecules.[34] As a comparison, the Al13 cluster was also used as adsorptive of **2PyNI**. The generalized gradient approximation functional by B88 exchange and LYP correlation (GGA-BLYP), along with a
35 double numerical plus polarization (DNP) basis set, was used for all the calculations. According to the result shown in Figure 6 the optimized **2PyNI**-Au13 system had no significant interaction and kept a distance of Au-N about 0.509 nm, the original value predetermined between Au and pyridine group. However, the
40 optimized **2PyNI**-Al13 had a strong Al-N interaction, in which the distance of Al-N was close to 0.2 nm.
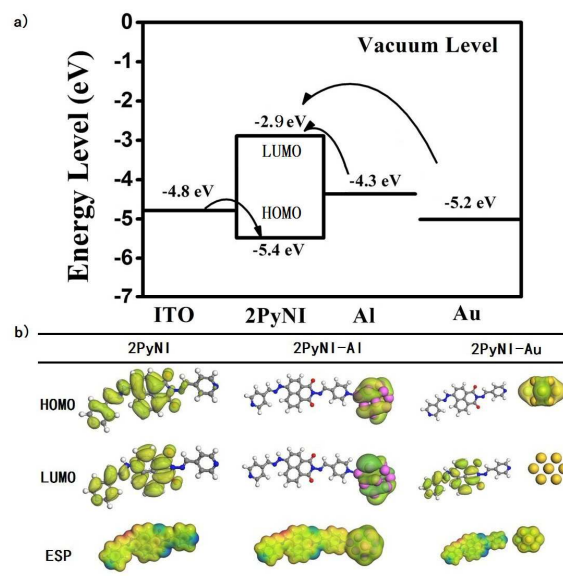
Figure 6. (a) Energy level diagram of HOMO and LUMO for **2PyNI**, the work functions of ITO, Al and Au electrodes; (b) Simulated highest
45 occupied molecular orbital (HOMO), lowest unoccupied molecular orbital (LUMO) and electrostatic potential (ESP) plots of 2PyNI.

The energy level diagram showed that as a negative bias was applied, the electron injection from the Al electrode to the LUMO of **2PyNI** was easier than the Au electrode. This result
50 corresponded to the test that the turn-on voltage of device **2** was lower than device **1**.

According to the calculation, **2PyNI** molecule itself contained some negative ESP zone (blue) forming charge traps (acceptor side). As the voltage increased, the traps were filled and then the
55 device turned to ON-state, showing bistable conductivity states. To device **1**, as the voltage was applied, the charge injected into the **2PyNI** film from the ITO and the electron transmitted from the HOMO to the LUMO of **2PyNI** and device **1** turned to ON-state. As the **2PyNI** had no interaction with the Au, the electron
60 hopped to the Au electrode and then the device returned to OFF-state showing volatile memory behavior.

To device **2**, as the voltage was applied, the electron transmitted to the LUMO from the HOMO level and then the device turned to ON-state. As the organic layer had strong interaction with Al, the
65 charge was trapped in **2PyNI** molecule and could not be recovered after removing the voltage. Thus, device **2** showed WORM characteristic.
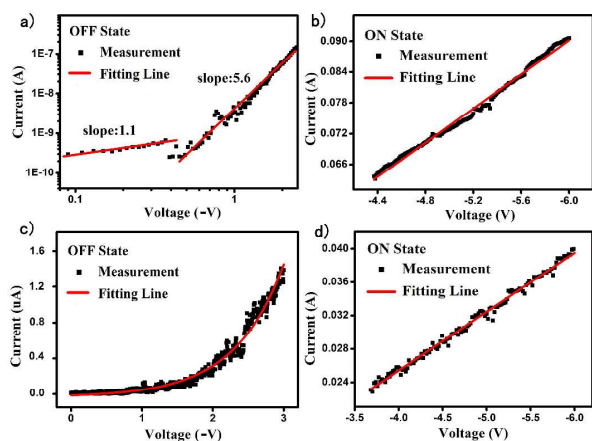
Figure 7. Analysis of Current-voltage characteristics of the (a) OFF-state with trap-limited space charge limited current (SCLC) model and (b) ON-state based on device 1; (c) OFF-state with the space-charge-free Frenkel Poole emission current model and (d) ON-state based on device 2.

To fur research these memory behaviours, we analyzed the I-V characteristics in detail with various conduction models. The Ohmic contact model was found to be matched with the I-V data for the ON-state of devices **1** and **2** (Figure 7b, d).[35-37] The results indicated that Ohmic conduction was dominant for all devices in the ON-state.

To device **1**, the I-V data of the OFF-state could be fitted by the trap-limited space-charge limited conduction (SCLC) model.[38-40] As shown in Figure 7a, the logarithmic plot of the I-V data for the OFF-state contained two linear regions for <0.46 V and >0.46 V, with slopes of 1.1 and 5.6, respectively. To device **2**, the I-V data of the OFF-state can be fitted by the space-charge-free Frenkel Poole emission current model.[41] The different conduction models showed different interaction between **2PyNI** and Au or Al.
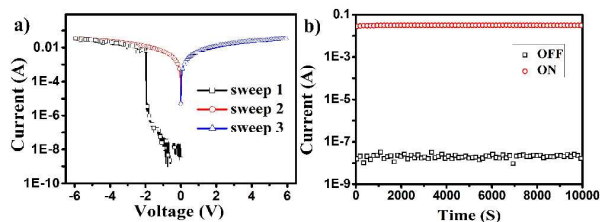
Figure 8. (a) Current-voltage characteristics of device ITO/**2PyNI**/MoO$_3$/Al; (b) The effect of retention time of the memory device ITO/**2PyNI**/MoO$_3$/Al under a constant stress of -1.0 V.

To block the interaction between **2PyNI** molecule and Al, we fabricated device ITO/**2PyNI**/MoO$_3$/Al. With the blocking layer MoO$_3$ thick of 5 nm, the device ITO/**2PyNI**/MoO$_3$/Al also showed WORM characteristic with lower turn-on voltage of -2.0 V compared with device **2** (Figure 8a). To device ITO/**2PyNI**/MoO$_3$/Al, the charge was also trapped in **2PyNI** molecule and could not return. Thus, device ITO/**2PyNI**/MoO$_3$/Al also showed WORM characteristic. The MoO$_3$ was conducive to the electron injection and therefore

decreased the switching voltage of device.[42-44] The approach of adding MoO$_3$ into device would provide a new method for decreasing turn-on voltage of electrical memory device.

Besides, the temperature dependence (between 250 and 320 K) of the current for ON state of device **1** and **2** were measured (Figure S7). It was found that the ON state of device **1** and **2** was weakly affected by the temperature, which excluded the formation of the metal bridge during the ON state. As the temperature dependence was very weak and there was a linear I-V characteristics, the tunneling effect might have dominated the ON-state.[45]
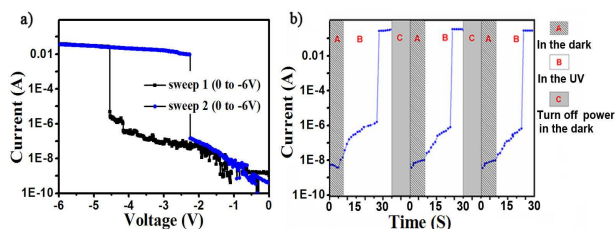
Figure 9. (a) Current–voltage (I–V) characteristics of device 1 lighted by 365 nm UV; (b) the electro-optical performance of the device 1.

The aromatic hydrazone group was photo sensitive as suggested by previous reports.[46,47] Device **1** showed no obvious change under irradiation of incandescent lamp. However, under the irradiation of the UV lamp (365 nm), the threshold voltage of device **1** was decreased dramatically from -4.3 V to -2.2 V (Figure 9a). When the voltage was fixed at -3.0 V (Figure 9b), for the first 8 s, the device **1** was in the OFF state in the dark. After being exposed to UV light (365 nm) for about 20 s, device **1** switched to ON state.

The UV–Vis absorption spectra of the **2PyNI** film before and after irradiation had showed no obvious change, which indicated the unchanged electronic transit. We tentatively assigned it to the polarity of hydrazone group. As the UV lamp (365 nm) was irradiated, the polar molecule **2PyNI** adsorbed the energy, beneficial for the charge separation and formation of ion channel. Therefore, the device **1** was inclined to be switched on a much lower voltage under the UV light. The electro-optical performance of device **1** could be repeated after being placed in the dark for a while, which showed potential application in UV sensor.

Conclusion

In summary, a small molecule **2PyNI** containing hydrazone group was synthesized and fabricated as an electro-active layer of the sandwich-structure memory devices. Through changing the top electrodes, we obtained different memory types. Device **1** with Au as top electrode showed volatile memory effect, while device **2** with Al as top electrode showed non-volatile WORM effect. The difference was assigned to the different interaction between metal and organic layer. Therefore, the interface of electrode and active film might play an important role in the memory performance in this case. It would provide useful information for tuning memory types by molecular design.

Notes and references

[a] Key Laboratory of Organic Synthesis of Jiangsu Province, School of Chemistry, Chemical Engineering and Materials Science, Soochow University (DuShuHu Campus), 199 Ren'ai Road, Suzhou, 215123, China
[c] Jiangsu Key Laboratory of Carbon-Based Functional Materials & Devices, Institute of Functional Nano & Soft Materials (FUNSOM), Soochow University (DuShuHu Campus), 199 Ren'ai Road, Suzhou, 215123, China

1 B. Cho, J. Yun, S. Song, Y. Ji, D. Kim, T. Lee, *Adv. Funct. Mater,* 2011, **21**, 3976.
2 S. L. Lian, C. L. Liu, W. C. Chen, *Appl. Mater. Interfaces*, 2011, **3**, 4504.
3 J. P. Wang, *Nat. Mater*, 2005, **4**, 191.
4 M. Colle, M. Buchel, D. M. Leeuw, *Organic Electronics,* 2006, **7**, 305.
5 J. C. Scott, L. D. Bozano, *Adv. Mater,* 2007, **19**, 1452.
6 P. Y. Gu, F. Zhou, J. K. Gao, G. Li, C. Y. Wang, Q. F. Xu, Q. C. Zhang, J. M. Lu, *J. Am. Chem. Soc,* 2013, **135**, 14086.
7 S. ChandraKishore, A. Pandurangan, *RSC Adv.,*2014, **4**, 9905.
8 C. Jin, J. Lee, E. Lee, E. Hwang, H. Lee, *Chem. Commun.*, 2012, **48**, 4235.
9 I. A. Hummelgen, N. J. Coville, I. Cruz-Cruz, R. Rodrigues, *J. Mater. Chem. C*, 2014, **2**, 7708.
10 A. D. Yu, T. Kurosawa, Y. H. Chou, K. Aoyagi, Y. Shoji, T. Higashihara, M. Ueda, C. L. Liu, W. C. Chen, *ACS Appl. Mater. Interfaces*, 2013, **5**, 4921.
11 G. Wang, S. F. Miao, Q. J. Zhang, H. F. Liu, H Li, N. J. Li, Q. F. Xu, J. M. Lu, L. H. Wang, *Chem. Commun,* 2013, **49**, 9470.
12 A. D. Yu, C. L. Liu, W. C. Chen, *Chem. Commun,* 2012, **48**, 383.
13 E. Kapetanakis, A. M. Douvas, D. Velessiotis, E. Makarona, P. Argitis, N. Glezos, P. Normand, *Adv. Mater,* 2008, **20**, 4568.
14 Q. D. Ling, D. J. Liaw, C. X. Zhu, D. S. H. Chan, E. T. Kang, K. G. Neoh, *Prog. Polym. Sci,* 2008, **33**, 917.
15 N. G. Kang, B. Cho, B. G. Kang, S. Song, T. Lee, J. S. Lee, *Adv. Mater,* 2012, **24**, 385.
16 Q. D. Ling, D. J. Liaw, E. Y. H. Teo, C. Zhu, D. S. H. Chan, E. T. Kang, K. G. Neoh, *Polymer,* 2007, **48**, 5182.
17 R. Zazpe, P. Stoliar, F. Golmar, R. Llopis, F. Casanova, L. E. Hueso, *APPLIED PHYSICS LETTERS*, 2013, **103**, 073114.
18 S. H. Hong, O. Kim, S. Choi, M. Ree, *APPLIED PHYSICS LETTERS*, 2007, **91**, 093517.
19 S. G. Hahm, T. J. Lee, D. M. Kim, W. Kwon, Y. G. Ko, T. Michinobu, M. Ree, *J. Phys. Chem. C*, 2011, **115**, 21954.
20 R. M. Duke, E. B. Veale, F. M. Pfeffer, P. E. Krugerc, T. Gunnlaugsson, *Chem. Soc. Rev,* 2010, **39**, 3936.
21 D. Kolosov, V. Adamovich, P. Djurovich, M. E. Thompson, C. Adachi, *J. AM. CHEM. SOC,* 2002, **124**, 9945.
22 Z. Ma, W. Sun, L. Z Chen, J. Li, Z. Z. Liu, H. X. Bai, M. Y. Zhu, L. P. Du, X. D. Shi, M. Y. Li, *Chem. Commun,* 2013, **49**, 6295.
23 N. R. Chereddy, K. Saranraj, A. K. Barui, C. R. Patra, V. J. Rao, S. Thennarasu, *RSC Adv.*, 2014, **4**, 24324.
24 G. Wang, S. f. Miao, Q. J. Zhang, H. F. Liu, H. Li, N. J. Li, *Chem. Commun,* 2013, **49**, 9470.
25 H. Kanno, R. J. Holmes, Y. Sun, S. Kena-Cohen, S. R. Forrest, *Adv. Mater.* 2006, **18**, 339.
26 S. L. Lim, N. J. Li, J. M. Lu, Q. D. Lin, C. X. Zhu, E. T. Kang, K. G. Neoh, *ACS Appl. Mater. Interfaces,* 2009, **1**, 60.
27 K. H. Kim, S. Y. Bae, Y. S. Kim, J. A. Hur, M. H. Hoang, T. W. Lee, M. J. Cho, Y. Kim, M. Kim, J. II. Jin, S. J. Kim, K. Lee, S. J. Lee, D. H. Choi, *Adv. Mater*, 2011, **23**, 3095.
28 Y. Ma, X. Cao, G. Li, T. Wen, Y. Yang, J. Wang, S. Du, L. Yang, H. Gao, Y. Song, *Adv. Funct. Mater,* 2010, **20**, 803.
29 S. F. Miao, H. Li, Q. F. Xu, N. J. Li, J. W. Zheng, R. Sun, J. M. Lu, C. M. Li, *J. Mater. Chem,* 2012, **22**, 16582.
30 H. Li, N. J. Li, H. W. Gu, Q. F. Xu, F. Yan, J. M. Lu, X. W. Xia, J. F. Ge, L. H. Wang, *J. Phys. Chem. C,* 2010, **114**, 6117.
31 C. J. Chen, H. J. Yen, Y. C. Hu, G. S. Liou, *J. Mater. Chem. C*, 2013, **1**, 7623.
32 Y. Q. Li, R. C. Fang, A. M. Zheng, Y. Y. Chu, X. Tao, H. H. Xu, S. J. Ding, Y. Z. She, *J. Mater. Chem.*, 2011, **21**, 15643.
33 B. Delley, *J. Chem. Phys*, 2000, **113**, 7756.
34 Y. Shichibu, K. Konishi, *Small*, 2010, **6**, 1216.
35 J. Hsu, Y. Chen, T. Kakuchi, W. C. Chen, *Macromolecules*, 2011, **44**, 5168.
36 B. Zhang, T. Cai, S. Li, X. Zhang, Y. Chen, K. Neoh, E. T. Kang, C. Wang, *J. Mater. Chem. C*, 2014, **2**, 5189.
37 L. M. Chen, Z. Xu, Z. Honga, Y. Yang, *J. Mater. Chem*, 2010, **20**, 2575.
38 T. J. Lee, S. Park, S. G. Hahm, D. M. Kim, K. Kim, J. Kim, W. Kwon, Y. Kim, T. Chang, M. Ree, *J. Phys. Chem. C*, 2009, **113**, 3855.
39 W. Kwon, B. Ahn, D. Kim, Y. Ko, S. GyuHahm, Y. Kim, H. Kim, M. Ree, *J. Phys. Chem. C*, 2011, **115**, 19355.
40 G. Tian, D. Wu, L. Shi, S. Qi, Z. Wu, *RSC Adv*, 2012, **2**, 9846.
41 G. Liu, Q. Ling, E. Y. H. Teo, C. X. Zhu, D. S. Chan, K. Neoh, E. T. Kang, *ACS NANO*, 2009, **37**, 1929.
42 H. Bronstein, J. M. Frost, A. Hadipour, Y. Kim, C. B. Nielsen, R. S. Ashraf, B. P. Rand, S. Watkins, I. McCulloch, *Chem. Mater*, 2013, **25**, 277.
43 Y. L. Chen, C. Y. Chang, Y. J. Cheng, C. S. Hsu, *Chem. Mater*, 2012, **24**, 3964.
44 S. L. Lim, N. J. Li, J. M. Lu, Q. D. Lin, C. X. Zhu, E. T. Kang, K. G. Neoh, *ACS Appl. Mater. Interfaces,* 2009, **1**, 60.
45 W. L. Leong, N. Mathews, B. Tan, S. Vaidyanathan, F. Dötz, S. Mhaisalkar, *J. Mater. Chem*, 2011, **21**, 5203.
46 H. Li, N. J. Li, R. Sun, H. W. Gu, J. F. Ge, J. M. Lu, Q. F. Xu, X. W. Xia, L. H. Wang, *J. Phys. Chem. C*, 2011, **115**, 8288.
47 S. S. Razi, R. Ali, P. Srivastava, M. Shahid, A. Misra, *RSC Adv*, 2014, **4**, 16999.